Visibility of Turbulent Ship Wakes in Dual-Polarized RADARSAT-2 Imagery

Daniel M. Roy and James K.E. Tunaley

***Abstract*---The observations of ship wakes in RADARSAT-2 Synthetic Aperture Radar fine beam mode images are described. Wakes were observed in about 50 percent of cases where ship detection was accompanied by an Automatic Identification of Ships (AIS) report. These were mostly turbulent wakes. The goal of the research was to understand the physical mechanisms and the factors involved in the visibility of turbulent wakes and to determine the potential of these wakes for classifying ships. It was found that wakes were visible only for small and moderate wind speeds less than about 6 m/s and that the visibility of bright arms was consistent with hydrodynamic modulation of the capillary waves responsible for radar Bragg backscatter. The modulation appears to be associated principally with swirling and linear surface flows due to propeller action; these cause compression and dilation of the waves. The characteristics of wakes from single screw vessels are partly determined by the sense of rotation of their propeller. This could be useful for cross-validation and classification purposes.**

***Index Terms*---Ship wake, turbulent wake, SAR, RADARSAT-2, polarimetric SAR, swirling wake, propeller wake.**

I. Introduction

SATELLITE RADAR can provide day-night wide area ship detection capability over maritime approaches including Arctic waters [1]. In a high resolution image, for example from the C-band Synthetic Aperture Radar (SAR) aboard RADARSAT-2, the ship return appears as a bright area. One problem is that, even with the large swath widths that can be achieved, the operational capability is limited by an insufficient number of satellites that is needed for persistent surveillance. Moreover, analysis of the radar bright return typically provides only accurate location of each ship as the satellite passes over it. The length of the ship is a useful parameter but can usually only be estimated approximately.

Self-reporting such as Automatic Identification of Ships (AIS) can be a primary source of information, at least in coastal regions, because AIS signals are transmitted by a moving ship every few seconds. Therefore a ship can be tracked. The role of satellite radar detections is to validate AIS information, which can be corrupted or "spoofed". Dynamic AIS data derived from a ship's transponder contains information about the identity of the ship, its course and speed and its position. Static AIS information is transmitted less frequently and includes the actual ship name, its dimensions, destination, and cargo information.

When ship wakes are observed in SAR images, they can sometimes yield an independent estimate of the ship's course and its speed. This information can also be used to validate the AIS data. However, the use of ship wakes in operational maritime surveillance requires that radar wakes are fully understood. This understanding includes the factors involved in wake visibility and the physical mechanisms responsible for them. Otherwise it is difficult to model and to assess advantages against costs and resources. Also it would be useful to know if wakes could add useful information that could assist in classifying a ship. A preliminary program was undertaken at the Royal Military College, Kingston, Ontario, to answer the fundamental questions.

The visibility of a ship wake in a SAR image involves the hydrodynamics of wake production, the physics of radar backscatter from the ocean surface and the signal processing of the SAR signal. Individually these can be considered to be moderately well understood but, because three fields of study are involved, there remain aspects of SAR ship wake images that are uncertain.

There are several types of hydrodynamic wake and it is necessary to consider these to avoid confusion that might arise because different wakes can exhibit similar features. Perhaps the most familiar wake class is the Kelvin wake of surface gravity wave wakes in deep water [2]. This is a pattern of waves that moves along with the ship. It comprises transverse waves, which propagate at angles between 0° and about 35.3° to the ship's track, and divergent waves, which propagate at angles in the remaining range up to 90° to the ship's track. Both sets of waves coalesce at the edges of the wake forming caustics of cusp waves. The half angle of the wake is about 19.5°. The Kelvin wake angle is fixed and the crest pattern does not depend on ship speed except for a scale factor; the ship speed affects the wavelength of the waves and so the Kelvin wake can be used to estimate both course and speed.

In shallow water the speed of propagation of a wave is limited to a maximum value related to the depth. When the ship is moving at less than the maximum speed, the wake crest pattern resembles that of the Kelvin wake but the half angle is greater than 19.5°. When the speed of the ship exceeds the maximum wave speed, the wake edge resembles a two-dimensional version of the Mach cone of a supersonic airplane. Inside the wake, there are only divergent waves and transverse waves are absent.

The Kelvin wake and its shallow water version are produced as the ship pushes water aside. In the reference frame of the ship, the disturbance is stationary and this fact is responsible for the stationarity of the crest pattern in the ship frame. However, other excitations can vary with time in the ship frame [2]. These include excitations due to ship motion (heave, pitch, etc.), propeller action and the reflection of ambient waves from the hull. Some excitations are narrow band, such as the effect of the propeller, which occurs at the blade frequency. Another example of a narrow band excitation is the reflection of swell waves from the hull. Other unsteady excitations can be broad band but with a peak at some frequency. In all cases the wake half angle can lie between 0° and 90°. When the excitation frequency and the ship

Published March 2010 and with minor corrections December 31st, 2010.

speed are high, the wake tends to be narrow. In some circumstances, this mechanism might be responsible for the narrow-V wake class. A narrow-V wake typically consists of two bright arms.

Internal gravity waves are produced when a ship moves in a stratified ocean where the density changes with depth. The changes in density occur as a result of temperature and salinity variations. For example, in the Strait of Georgia, a layer of fresh water from the Fraser River can overlie salt water. Waves on the internal interface can manifest themselves at the surface in the form of flow velocity fluctuations and produce a wake in a SAR image. The crest pattern of an internal wave wake is narrow and typically resembles that of a shallow water wake. Because the maximum velocity of internal waves is usually less than 2 m/s, the wake typically comprises only divergent waves.

The viscosity of water is finite and water sticks to the surface of a ship hull. A moving ship creates a thin boundary layer in which the water velocity changes rapidly from the hull to the edge of the layer, where it moves at a velocity consistent with potential flow. Potential flow represents the flow that would occur if water had zero viscosity and did not wet the hull. Near to the bow in the boundary layer, there could be a region of laminar flow but in practice laminar flow soon gives way to turbulent flow and at the stern the boundary layer is strongly turbulent. Beyond the stern, the boundary layer is detached from the ship and comprises a mean linear flow component in the direction of the ship and a turbulent component. Because the ship exerts a force on the water to set it in forward motion, the water exerts an equal and opposite force on the ship resulting in viscous hull resistance. As well as a drag component tangential to the hull there is a pressure drag due to the wake at the stern, which reduces the stern pressure.

To overcome the drag on the ship and to cause it to move at constant velocity, the propeller accelerates water through the propeller disk and produces a thrust. This creates another similar horizontal column of water but moving away from the ship. Again this column is turbulent and carries linear momentum. However, the wake from a normal propeller also carries a swirling component or angular momentum.

In both the viscous hull wake and the propeller wake, turbulent eddies entrain water at the edge of the wake and the wake broadens. The broadening is accompanied by a reduction in both the mean and turbulent flow components but this occurs very slowly and results in a long wake lasting up to tens of kilometers astern.

Radar signals are backscattered efficiently from a rough ocean surface when the wave vector of capillary waves matches the radar wavelength according to the Bragg condition [4,5]. These "Bragg" waves propagate on the sea surface either directly towards the radar or away from it. The theory of scattering is based on the assumption that the waves have amplitudes that are small compared to the wave length. This is usually not satisfied and leads to a two scale theory in which capillary waves ride on large scale ocean waves. Thus the large scale waves result in variations of the local angle of incidence, which affects the scattered amplitude directly as well as the wavelength from the Bragg condition. The effect is described as "tilt modulation" and is partly responsible for the visibility of ocean waves in SAR images. The orbital velocity of large scale waves also tends to compress or dilate capillary waves, which gives rise to an effect called "hydrodynamic modulation". Hydrodynamic modulation can be complicated because it is often a non-linear process involving a change in wave frequency, a transformation of the Bragg domain in wave vector space, a shift in the capillary wave spectrum, attenuation and energy exchange between wave and fluid.

In addition to Bragg scattering there may be significant contributions to the backscatter coefficient by specular reflections at angles of incidence less than 30° including contributions from wave cusps and from breaking waves.

The processing of the raw SAR signal utilizes the Doppler history of targets to derive along-track position in an image. It is based on the assumption that a target is stationary on the earth's surface. When the target has a component of velocity in the radar direction, the processor interprets this as a shift in along-track position so that the target is shifted in the image plane in the azimuthal or along-track direction. This is known as "velocity bunching" because it can render ocean waves visible by compressing or dilating the returns preferentially into certain regions of the image. One important consequence of velocity bunching is that a ship is usually displaced in a SAR image whereas the wake appears in more or less the correct position. Any surface flow including orbital flows from ambient and wake waves as well as turbulent wake flows are likely to introduce velocity bunching.

Ship wakes in SAR imagery have been described by many authors. Case et al [3] analyzed images from Seasat, which carried a SAR operating at L-band with HH polarization. They observed Kelvin, narrow-V and turbulent wakes. The focus of their work was an explanation of narrow-V wakes, which can be seen mainly when the ship is traveling at angles close to the SAR track and at low angles of incidence.

A preliminary study of the propeller and its effect on wakes in SAR images was described by Buller and Tunaley [6] and by Tunaley et al [7].

Peltzer et al [8] studied the wake of a twin hulled ship, the USNS Hayes, using a thermal infrared scanner, X-band radar and an airborne camera. They found that turbulent motions within the wake and the addition of surface films reduced the radar backscatter by attenuating existing capillary waves and suppressing the creation of new waves by the wind. However, they did not suggest that the dark turbulent wake in a SAR image was solely due to surfactants.

Lyden et al [9], Skoelv [10,11], Skoelv and Wahl [12] and Skoelv et al [13] describe comparisons between SAR imagery of ship wakes from airborne SAR and Seasat and a theory based on the Swanson [14] model of vortex production. In this model, the ship produces twin vortices at the stern and these cause surface flows that result in hydrodynamic modulation. It turns out that this type of mechanism is consistent with the results obtained in this study except that in our case the flows are mainly associated with propeller wakes.

Skoelv [15] analyzed a large database of about 800 ships and wakes from the ERS satellite. Over half the ships were accompanied by dark turbulent wakes. However, unlike the present study, there were few turbulent wakes with bright arms.

Reed and Milgram [16] based their explanation of the dark turbulent wake on the redistribution of natural surfactants.

Hennings et al [17] dealt mainly with Kelvin wake visibility. They created backscatter models based on tilt and hydrodynamic modulation that provided estimates of cusp wave visibility as a function of SAR wavelength, polarization and incidence angle. The principal imaging mechanism was tilt modulation. The models were supported by over 100 ship wake signatures. Their work shows that RADARSAT-2 fine beam VV parameters are not well suited to cusp wave visibility.

Melsheimer et al [18] analyzed about 400 SAR wakes and 100 optical wakes. The SAR wakes were from ERS-1 and -2, both of which carry C-band radar with VV polarization; incidence angles typically lie in the range 20° to 26°. The optical satellite was SPOT. They found that at least one component of the Kelvin wake could be seen in 17% of the SAR wake images but that a turbulent wake was visible "in all investigated cases". Visibility of the Kelvin wake was attributed to tilt modulation and the dark turbulent wake to the effects of turbulent vortices. Bright edges of the turbulent wake were stated to be due to the compression of surface films by the swirling propeller flows.

II. Ship Characteristics

To compensate for the influence of the water and air, which tends to resist the forward motion of the ship, the vessel must be propelled forward and this is usually by means of rotating propellers. Most large merchant ships are driven with a single propeller but, where maneuverability is important, the ship is propelled by twin screws Twin screws are often found on tugs, ferries and military vessels. The presence of bow and stern thrusters, which are used for docking is not relevant here.

On vessels with a single screw, older literature states that the sense of rotation is almost invariably right handed [19,20]. This means that its rotation is clockwise when looking from astern. The clockwise rotation implies that the swirling component of the wake induces a component of surface flow towards the starboard side of the ship. However, it is likely that left-handed screws are more common in builds after 2000.

A notable case is the double-ended ferry. This has a propeller at each end so that cars can load or disembark without turning the ship around when it reaches port. The C-class used by BC ferries is an example [21] and these ships use Controllable Pitch Propellers (CPPs). One of the screws is right-handed and the other is left-handed. The screw at the end of the ship acting as the bow may be disengaged and feathered, which means that its blades are oriented for minimum drag. The screws are engaged through a gearbox to engines using hydraulic clutches and the engines are run continuously at constant speed even in port. If the ship is driven by its left-handed propeller, the surface flow in the wake will be towards the port side.

Twin screws are always counter rotating, i.e. one is right and the other left handed. Otherwise "propeller walk" causes serious problems in steering the ship. The rotations are usually such that the surface flows are outwards and this can be expected for almost all civilian ships. In some cases, there may be an advantage to having inward flows to enhance maneuverability and this characterizes some military vessels.

Contra-rotating screws are used occasionally. These are propellers on the same axis that rotate in opposite directions. The concept is that the aft screw runs in the swirling wake of the forward screw and recovers energy from the swirl. To a first approximation the swirl downstream is eliminated. Though contra-rotating screws are more efficient, this is offset by their additional manufacturing and maintenance costs.

Resistance to ship motion or drag has three principal components. The first is due to wave making. The Kelvin wake and other surface or internal gravity wave wakes carry energy and momentum; the energy and momentum must be supplied ultimately by the ship's engines. Clearly wave production creates a force on the ship's hull, which can be categorized as wave making drag. According to Comstock [22] the main component of this varies as the ship speed, U, to the sixth power. It dominates the drag at high speeds.

The second component is hull drag associated with viscosity. To understand this we can imagine that any waves on interfaces (air-water or internal) are suppressed. The viscous hull forces can be estimated from experiments on rough planks (originally carried out by Froude), as summarized by a variety of empirical formulae [22]. For a turbulent boundary layer the drag coefficient can be estimated in terms of the Reynolds number, which depends on the kinematic viscosity, the ship speed and the length of the ship; the Reynolds number usually lies between 10^7 and 10^9.

The viscous hull resistance must be augmented by form drag associated with the decrease in dynamic pressure around the stern due to detachment of the boundary layer. The decrease causes water to move into the stern area in the form of eddies and adds to the wake turbulence. The form drag can vary from 5% to 15% of the viscous drag in warships and up to 40% for merchantmen [22].

Air resistance is generally small. According to [22], Admiral Taylor suggested that the resistance in a head wind can be estimated by treating the ship as a flat plate of area $B^2/2$ (B is the beam) with an appropriate drag coefficient. In light winds, air resistance amounts only to a few percent of the viscous hull drag.

Small craft are often used for smuggling or piracy. These may be constructed of wood or fiberglass and their radar cross-sections are small by virtue of their size and construction. They cannot usually be detected in satellite radar imagery by returns from their hull. They are often high speed planing boats known as "go-fast" or "cigarette" boats with a power-boat racing hull; their speed can exceed 60 knots. The high power required for such speeds may produce a visible radar wake and allow detection.

III. Turbulent Wake

The turbulent wake is usually considered in terms of mean and fluctuating fluid flow components. The mean flows can be both linear and swirling angular flows. The mean flow in the wake from the viscous hull drag is in the direction of the ship and extends over the cross-section of the ship at the stern. The mean flow in the propeller wake contains both linear and angular components and its cross-section near the stern is of the order of the propeller disk; the propeller wake is embedded within the viscous hull wake.

The theory of turbulence continues to receive much attention because the evolution of a fluid parcel depends on non-local characteristics at any given time. Moreover, the motion appears

to be chaotic. To overcome these problems, Prandtl introduced the mixing length approach in which turbulence is treated as a random process of diffusion but the diffusion coefficient is a function of the solution [23]. The diffusion of a gas is characterized by a mean free path and the velocity of molecules. In Prandtl's theory, the mean free path is replaced by the mixing length, which in this case is of the order of the wake diameter and the eddy velocity is of the order of the mean flow velocity.

Even with this model, the solution of a problem can be difficult unless the problem is simple. There are several special or canonical cases that have been discussed in the literature. These are the linear-momentum wake, the angular-momentum wake and the zero-momentum wakes. The viscous hull wake corresponds to the linear-momentum wake, while the propeller wake is a combination of the linear- and angular-momentum wakes. As will be explained below, the zero-linear-momentum wake and the zero-angular-momentum wake are not expected to be relevant in the present context.

In the canonical cases, wakes in three dimensions are assumed to be axisymmetric and the presence of a free surface is neglected. In the far wake regime, the theory of axisymmetric wakes is usually based on one of three approaches and it is assumed that the Reynolds number is very high so that inertial forces are much greater than viscous forces. The latter can then be ignored. The methods are often based on one or more of the following:

1. Prandtl's mixing length theory used directly.
2. The assumption of self-similarity, which implies that the solutions for the mean flows and other variables are similar at all distances behind the ship, z, except for scale.
3. Dimensional analysis applied to a simplified Navier-Stokes equation and an assumption that a quantity, such as linear momentum, is conserved.

Prandtl's method is illustrated by Schlichting [23], self-similarity by Birkhoff and Zarantonello [24] and dimensional analysis by Reynolds [25]. The methods give similar results.

Perhaps the simplest derivation involves the third approach. In the case of the viscous hull wake, the linear momentum of a length of the wake (in the ocean frame) is conserved because the net external force on it is zero. In the simplified equations, the only parameters relevant to the wake diameter, b, are the rate of momentum production, P', the ship speed, U, the water density ρ and z, the distance downstream. However these only occur in combinations z/U and $P'/(\rho U)$. Therefore we have purely on dimensional grounds:

$$b = \left(\frac{\beta P'(z - z_0)}{\rho U^2} \right)^{1/3} \qquad (1)$$

where β is a constant and z_0 is some origin determined by the wake dimensions close to the ship stern. It is found that the mean wake velocity varies as $z^{-2/3}$ and the Reynolds number, now based on the wake diameter and the mean flow velocity, goes as z^{-1}. These results imply that this type of wake can persist for a long distance behind the ship before dissipation at low Reynolds numbers becomes important.

The principal results of the three methods are given in Table 2 for four distinct cases. Here p is the exponent that represents how fast the wake width increases with distance astern, q is the exponent for the fluid speed and s is that for the Reynolds number (based on the wake width). The theory is very compelling because it relies only on simple concepts such as conservation laws and self-similarity.

TABLE 2
WAKE EXPONENTS

Wake Type	**p**	**q**	**s**
Linear-momentum	1/3	-2/3	-1/3
Angular-momentum	1/4	-3/4	-1/2
Zero-linear-momentum	1/5	-4/5	-3/5
Zero-angular-momentum	1/6	-5/6	-2/3

Experiments have been carried out in controlled conditions to study turbulent wakes. One difficulty is that the Reynolds numbers that can be explored in the laboratory are smaller by orders of magnitude that those that occur in practice. Therefore questions arise as to whether the laboratory turbulence truly represents that in a real ship wake and whether it is sufficiently strong for self-similarity to persist over long distances. Conversely, the failure of a laboratory experiment to confirm the theory does not necessarily invalidate it for very high Reynolds numbers.

Higuchi and Kubota [26] have conducted experiments on linear momentum wakes in the far field of an axisymmetric body and have verified the simple mixing length results. The Reynolds number based on body diameter was 27,000. The velocity profile across the far wake was close to Gaussian.

These authors also studied the zero-linear-momentum wake and found that, though self-similarity was attained, the centerline velocity fell off faster than predicted by the simple theory ($z^{-4/5}$). This was attributed to a failure of an assumption that eddy viscosity was constant.

Serviente and Patel [27] have examined the linear momentum wake from an axisymmetric model in its near field using Reynolds numbers (based on the body length, L) of about 10^6. They find that the mean velocity defect (the flow relative to the ocean) was self-similar after a distance given by $z/L > 0.4$; this condition defines the far wake. In the far wake, the velocity profile broadened as $z^{1/3}$ but the second moment of the velocity fluctuation decreased more slowly than the theory indicated over small values of z/L that were limited by the experimental arrangement. Within the experimental limitations, the results were consistent with the simple theory.

In another paper [28] these authors consider the zero-momentum wake. Self-similarity was achieved for $z/D > 12$ (D is the body diameter). It was found that a detailed description of the wake required several length scales and these varied differently. The centerline velocity was found to decrease more rapidly than the simple theory predicts as in [26] but the wake width indeed increased as $z^{1/5}$. The turbulent intensity measured by the variance of the velocity fluctuations fell as $z^{-8/5}$, as required by similarity theory. The data were compared with some of the original work of Naudascher [29]; there was a general agreement.

Further experiments were conducted by Serviente and Patel [30] for the zero-linear-momentum swirling wake. Their case of "strong swirl" corresponds to our angular-momentum wake,

which would be produced by a rotating paddle rather than a jet or propeller. Again multiple scales were needed for a full description. The work seems to imply that at least a partial approach to self-similarity occurred when z/D > 13. Results were consistent with the simple swirling wake theory in the far wake. However, the presence of both a linear jet and a body wake, though generating zero linear momentum, rendered interpretation more difficult than in the other cases.

Chernykh at al. [31] have modeled the zero-momentum wake and concluded that their numerical approach matched observations. Self-similarity was observed for large values of z/D in the range 100 to 1000 depending on the parameter. The distances were much larger than those in the Serviente and Patel experiments; this probably explains why these last authors did not observe self-similarity in the zero-linear-momentum wake.

The experiments suggest that the simple theory is adequate to explain the behavior of the far wake for the linear-momentum and the angular-momentum wakes because only one length scale is needed. In general, memory of the initial conditions that generated the wake tends to persist downstream. The simple theory for the other cases can be used directly if attention is restricted to the wake width, the mean flow and the variance of the turbulent fluctuations.

The application of the canonical results to a practical situation must take into account that the zero-momentum cases are very sensitive to the balance of momenta from the body wake and propeller jet [26].

In the case of surface displacement ships, with the exception of very small speeds, wave and air resistance are likely to be a significant proportion of the viscous hull drag. Therefore the wake will almost never fall into the zero-linear-momentum class. The torque from a single propeller is balanced by a slight heel; this shifts the ship's metacenter laterally relative to the ship's center of gravity. (The metacenter is a point through which the buoyancy force passes.) Thus the zero-angular-momentum wake is not appropriate. Twin propellers do not require a gravitational torque for compensation but a single axisymmetric model for the two wakes is not appropriate. In general only a combination of the linear-momentum and the angular-momentum models applied to each screw is pertinent. However, we note that a pure linear-momentum wake can be produced by a ship under sail.

IV. Wake Flow Estimation

The distribution of the mean velocity defect across the wake radius of a linear-momentum wake has been observed to be close to Gaussian as would be expected from a diffusion process. The constant β can be estimated from Schlichting's experiments on the wake behind a circular cylinder [23] and the rate of production of linear momentum can be estimated directly from the viscous drag from the hull and appendages augmented by the form drag; this is based on Newton's second law.

For a propeller wake, the rate of production of linear momentum depends on the shaft power at the propeller and the propeller efficiency. If required, this production can be related to the total drag, including wave making and air resistance. The flow in the angular momentum wake can be estimated by assuming that the mean angular velocity profile of the fluid is also Gaussian.

To appreciate the order of magnitude of these estimates, we apply the approach to the double ended ferry, the Queen of Alberni. The parameters for this ferry can be obtained from numerous sites on the Internet and are provided in Table 3. This ship has shallow screws; the blade tips are only just below the surface. From this table, estimates can be made for the ship traveling at its service speed in calm waters; a typical propeller efficiency of 60% is assumed [22] and the wave making plus air resistance are set equal to the net viscous drag.

TABLE 3
Queen Of Alberni Parameters

Parameter	**Value**
Length (m)	139
Maximum Beam (m)	27.1
Mean Draft (m)	5.5
Maximum Draft (Prop. Tip, m)	5.72
Block Coefficient (estimated)	0.6
Number of Propellers	1
Number of Blades	4
Propeller Shaft Depth (m)	3
Propeller Diameter (m)	5
Propeller Type	CPP
Service Speed (knots)	19
Propeller Speed @ 19 knots (rpm)	~170
Maximum Power (MW)	8.83

Fig. 1 shows the wake diameter as a function of distance astern. The linear momentum appears to dominate the wake evolution. It should be noted that the graph depicts the wake width under water and not the apparent width at the surface.

To estimate the surface flow velocities it is necessary to take into account the free surface. A simple approach is to introduce an image of the wake above the surface so that boundary conditions are satisfied, at least approximately. There are two effects. One is to double the horizontal velocities from their previous values. For swirl, another is to cause a small drift in the direction of the surface flow and a distortion of the angular momentum wake. These effects arise from the interaction of the wake with its image.

Fig. 2 shows the maximum horizontal *surface* velocities in the wake for the linear and angular momentum wakes; the effect of the free surface in causing drift and distortion is neglected. Close to the ship, the maximum surface flow velocity, which occurs directly above the propeller axis, is dominated by the angular momentum from the propeller. At greater distances, the wake evolution is dominated by the linear momentum wake. It is noteworthy that the maximum velocities can be much greater than the group velocity of capillary waves; the group velocity of Bragg waves appropriate to RADARSAT-2 radar signals in the fine beam mode is about 0.12 m/s. Therefore the model suggests that wake flows may strongly influence radar returns for long distances astern.

The accuracies of the rates of production of linear and angular momenta are believed to be adequate for this application even though the values of β affect the estimates in Figs. 1 and 2. The wake diameters are not sensitive to these because they are

raised to a small power, for example in equation (1). For the estimated velocities, close to the ship the dependence is mainly through the exponential terms in the Gaussian profiles but far from the ship the estimates are insensitive to these quantities. Thus, the character of the graphs and the relationship between the velocities due to swirl and those due to linear flow are insensitive to the parameters, varied within reasonable limits.

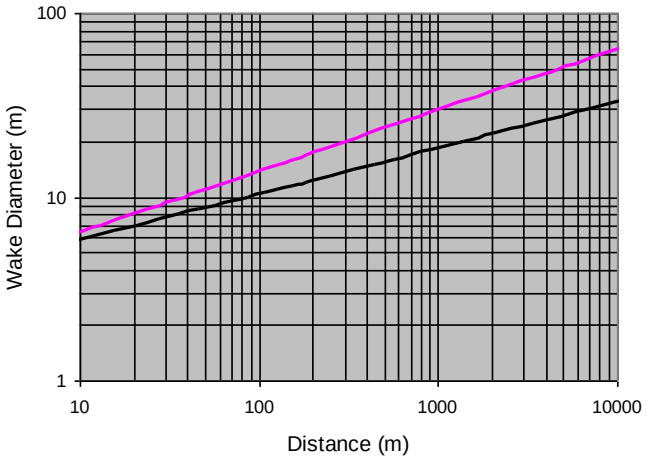

Fig. 1. Estimated wake diameters as a function of distance astern for angular momentum wake (—) and linear momentum wake (—) for the Queen of Alberni.

V. SAR Wake Imaging Processes

Radar backscatter from the sea surface arises from capillary waves that match the Bragg wave vector and from discrete features, such as breaking waves. It seems unlikely that the backscatter from a turbulent wake in a calm sea would involve reflection from discrete scatterers. However, at high wind speeds scattering from discrete areas could be associated with the ambient sea.

Because the spectrum of wind generated waves is very broad, the backscatter at C-band radar wavelengths only varies by a few decibels as a function of the angle between the principal direction of the capillary waves (which is typically in the direction of the wind) and the Bragg wave vector direction [32]. As noted, the Bragg wave vector direction is along the sea surface either towards or away from the radar.

Under low and moderate wind conditions and associated sea states relevant to the observation of radar wakes, tilt modulation is not very important. However, hydrodynamic modulation is expected to be a significant factor because of wake flows. Both mean and fluctuating flows in the wake can affect the generation and the propagation of capillary waves.

Propagation of capillary waves across a flow field over which the velocity varies will be subject to Doppler shift and refraction. It is important to note that wave energy is not conserved during the propagation from one region of the flow to another with different velocity. This is because work can be done on or by the wave on the flow itself; this changes the energy density in the wave. If viscous attenuation is negligible and the change in flow velocity changes over a wavelength is small, an adiabatic invariant, "wave action", is conserved along a ray.

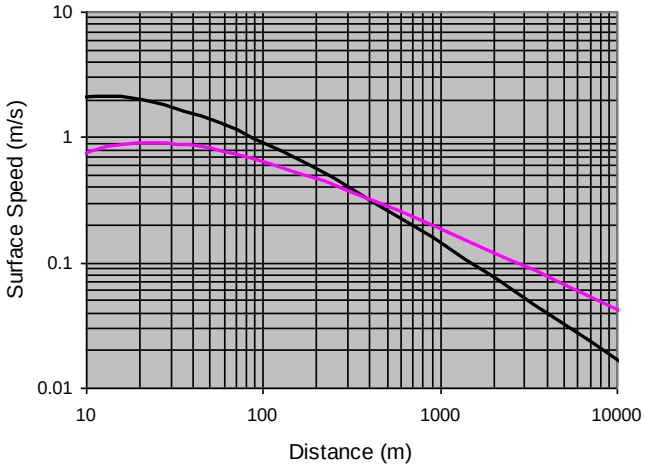

Fig.2. Maximum surface velocities in the propeller wake of the Queen of Alberni for angular momentum (—) and linear momentum (—) wakes.

The effect of wake flows can be broken down into several elements. Firstly the Bragg condition implies that the radar is only sensitive to backscatter from a small region in capillary wave vector space. The center of this is set at the Bragg wave vector and its dimensions are determined by the azimuthal and range resolutions of the radar. In the presence of surface flows, the Bragg waves at one position in the wake may be created at another position where the area of wave vector space, as determined for example by back tracing a ray, is different. This can occur through Doppler shifting.

For C-band radar and smaller wavelengths for which viscous attenuation is significant, the Bragg waves do not persist over distances longer than a few meters. However, at L-band wavelengths, the waves can persist over hundreds of meters for 1000 s or more, depending on the incidence angle. Therefore the wake mechanisms discussed by Case et al. [3] for Seasat are not relevant to RADARSAT-2.

VI. Experimental Approach

RADARSAT-2 images were ordered through the Canadian Space Agency. Fine beam mode dual polarization images were chosen in the Single Look Complex (SLC) format. A compromise was necessary between the high resolution needed to observe small wake features and the swath width needed to observe many ships and wakes. The fine beam mode images have a resolution of about 8 m and a swath width of about 50 km.

The desired resolution was dictated by the wavelength of the transverse waves of a Kelvin wake; the wavelength, λ_T, of transverse waves [2] is given by:

$$\lambda_T = 2\pi U^2 / g \qquad (2)$$

where g is the acceleration due to gravity. A ship traveling at 10 knots creates waves with a wavelength of 17 m. Therefore, according to the Nyquist criterion, a resolvable wake (without aliasing) can be observed only for ships moving at this speed or faster.

The areas over which imagery was taken were the approaches to Halifax Harbor, Lake Ontario near Kingston and the Strait of Georgia. The fine beam swath width was appropriate to these areas because the shipping routes tended to be concentrated in these areas. The areas were imaged between September 10th, 2008 and December 22nd, 2008.

Polarizations of VV and VH were chosen. The VV polarization ensured that the return from the ocean surface was much higher than the thermal noise generated in the radar receiver even for low wind conditions. When combined with the VV polarized imagery, the VH polarization provides an independent wake data source that reduces the effect of speckle noise and provides better contrast than either image alone.

Wind speeds (at 10 m height) and directions were obtained from Environment Canada websites. Information for Halifax was from a station on McNabs Island, for the Strait of Georgia it was from Sand Heads Point light and for Lake Ontario it was from Point Petrie.

Ground truth was provided by the Regional Joint Operations Centers on the east and west coasts in the form of AIS data. This was derived from Vessel Tracking Management Systems (VTMS). There was also an AIS receiving station at the Royal Military College, Kingston. AIS signals included the ship name, a ship identification number, the ship's position, and its speed and course. The system operates using a transponder system at VHF and is limited to line of sight. In practice it yielded signals from as far away as 40 km.

AIS is a form of self-reporting required by international law for ships of displacement greater than 300 tons. Although it cannot be considered to be totally reliable, the type of information needed for this study is usually correct and the data was adequate for its purpose [33].

The images were analyzed using the software packages PolSARPro and ENVI. These tools allow an operator to examine different combinations of polarimetric imagery and to utilize the geo-reference data included with RADARSAT-2 files.

The downloaded and uncompressed image folders were first imported into PolarSARPro, version 3.0, which is available from the European Space Agency. Denoting the VH complex pixel amplitude by h and the VV complex pixel amplitude by v, the following covariance matrix elements can be defined:

$$\begin{aligned} C_{11} &= < h^* h > \\ C_{12} &= < v^* h > \\ C_{21} &= < h^* v > \\ C_{22} &= < v^* v > \end{aligned} \tag{3}$$

where the angle brackets indicate integration over a small block of pixels. The color components of the composite image, displayed in units of decibels, were:

$$\begin{aligned} R &= C_{22} \\ G &= C_{11} + C_{22} - C_{12} - C_{21} \\ B &= C_{11} \end{aligned} \tag{4}$$

The PolSARPro composites were used to identify ships and wakes.

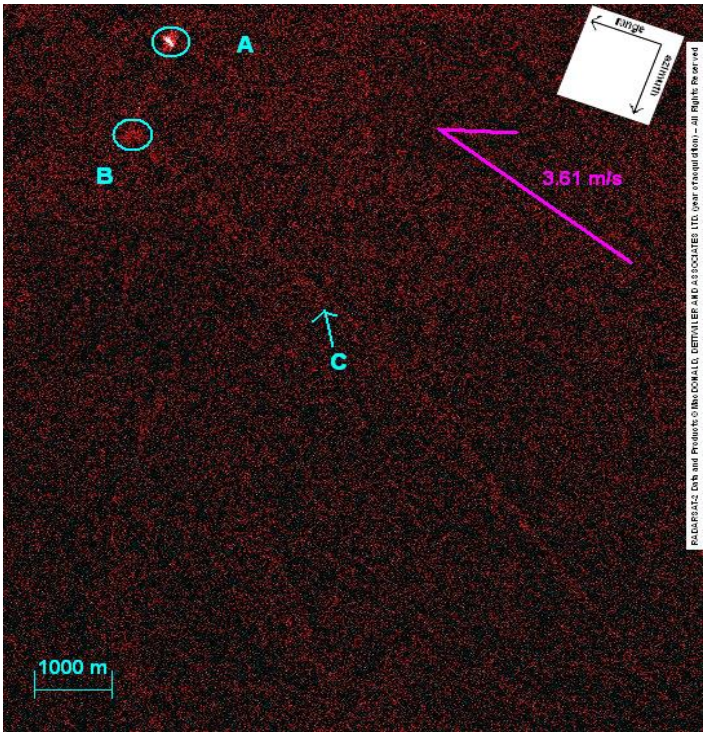

Fig. 3. Composite image shows Queen of Alberni ferry with a long turbulent wake. A: Ship return. B: Head of wake. C: Bright edge of turbulent wake to port.

To reduce speckle noise during the ship and wake detection process, a refined Lee filter was employed. This is an adaptive filter that smoothes background noise while preserving features in an image. The size of the mask was 7 pixels by 7 pixels.

The output files from PolSARPro were ingested into ENVI, which provides many image analysis tools, including geo-referencing based on the tie points included with a RADARSAT-2 image package. A subjective analysis revealed that a composite of the VV and VH images expressed as a Red-Green-Blue (RGB) image was near optimal for wake detection. An example from the Straits of Georgia is shown in Fig. 3. In this image the colors are determined by:

$$\begin{aligned} R &= C_{22} \\ G &= B = C_{11} \end{aligned} \tag{5}$$

Because the ship, the Queen of Alberni, was moving away from the radar, its image was displaced on the image plane in the azimuthal or cross-range direction. The magnitude of the displacement corresponds to its reported speed of 19 knots. The wake was about 10 km long and consisted of a dark region that became visible a few hundred meters astern. On the port edge of this dark turbulent wake was a narrow diffuse bright line.

VII. Results

A total of 60 ships were imaged and correlated with AIS data. Of these 31 exhibited a wake and 29 did not. There were no obvious Kelvin wakes observed though a further detailed analysis might reveal faint cusp arms. Two of the wakes were classified tentatively as narrow-V types (there was no evidence

of crest structures typical of internal waves) and the remaining 29 were classified as turbulent wakes.

A variety of ship types were seen ranging from tugs (17) and ferries (21) to large merchantmen (22). The smaller ships were mainly propelled by twin screws but the larger ships were propelled by a single screw. Some of the ferries had twin screws and some were double-enders.

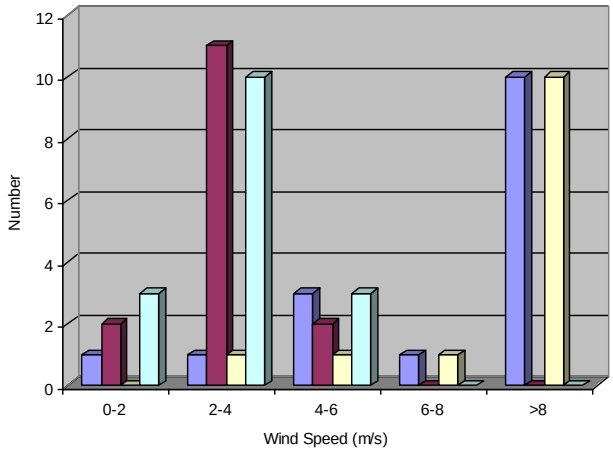

Fig. 4. Histogram of results showing wake visibility as a function of wind speed. Non-visible wake from single screw . Visible wake from single screw . Non-visible wake from twin screw .Visible wake from twin screw .

Fig. 4 summarizes the dependence of wake visibility on wind speed. Above a speed of 6 m/s, no wakes were observed. Below wind speeds of 6 m/s, wakes were observed for both single and twin propeller ships; the ratios of visible to non-visible wakes were 16:5 and 15:2 respectively. Though this suggests that twin screwed ships are more likely to be visible, a chi-squared test reveals that the data alone are insufficient to support this conclusion.

Fig. 5 is a plot of the fraction of visible wakes as a function of ship speed, combining the results from single and twin screwed ships. A linear trend line is included and the plot demonstrates that ship speed is a significant factor in wake visibility; ships traveling at speeds of greater than about 7 m/s are more likely to produce a visible wake than not. It should be noted that the plot includes all the observed wind speeds. The effect of wind speed is illustrated by Fig. 6. The fraction of visible wakes is shown when the wind speed was less than 6 m/s; there were 38 ships in this set. In this case most wakes were visible especially for those ships traveling at high speed. A linear trend line is included again.

The ship wake characteristics fell into five categories. These were:

- No visible wake,
- Wake comprising a dark line,
- Wake comprising one bright arm to starboard and a dark arm to port,
- Wake comprising one bright arm to port and a dark arm to starboard,
- Wake comprising two bright arms with a dark central area.

It should be noted that only one wake was observed that just consisted of a dark line (the ship Malaspina), though in a few cases a bright wake edge was faint.

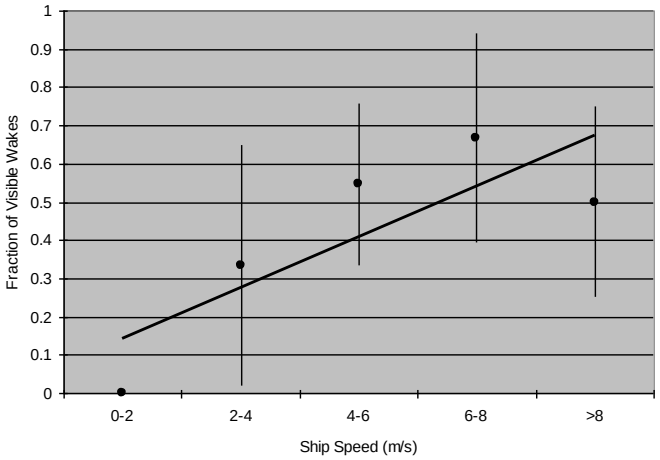

Fig. 5. Fraction of visible wakes as a function of ship speed. Error lines represent two standard deviations on either side. All wind speeds are included.

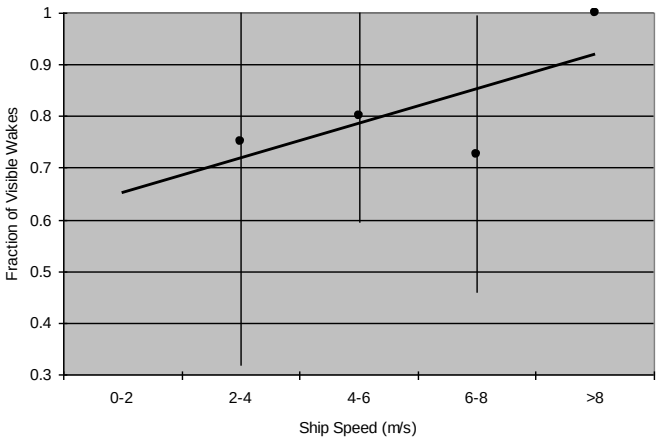

Fig. 6. Fraction of visible wakes as a function of ship speed for wind speeds less than 6 m/s. Error lines represent two standard deviations on either side.

Wake visibility is expected to depend on the geometry of the surface flows through hydrodynamic modulation. The modulation will be affected by the surface flow pattern from the screws and the wind direction relative to the ship course and the radar. It is necessary to examine the principal direction of the Bragg waves (towards or away from the radar) and the angle that these Bragg waves made with the expected flow vector. We note that the range direction of RADARSAT-2 at mid-latitudes was on the order of 10° from a line of latitude.

Table 4 provides data for the 7 ships for which no wake was visible and the wind speed was less than 6 m/s. 'A' and 'D' denote "Ascending" and "Descending" satellite passes, while LH indicates a confirmed left-handed screw. In the following, it is assumed that the swirl flow usually dominates wake visibility (see Fig. 2).

TABLE 4
SHIP, WIND AND GEOMETRIC PARAMETERS

Ship	Type	Length (m)	Draft (m)	Speed (m/s)	Screws	Ship (°T)	Wind (°T)	Pass
Algowood	Cargo	222	8.8	5.9	1 CPP (LH)	243	10	D
Polydefkis	Cargo	129	8.4	6.1	1	230	30	A
Stella Prima	Cargo	101	7.4	6.7	1	207	340	D
Blacky	Cargo	185	10.4	7.0	1	37	340	D
National Geographic Explorer	Passenger	112	4.6	6.0	1	0	340	D
Grand Mariner	Passenger	29	3.0	5.2	2	18	10	D
Hebron Sea	Cargo	78	6.6	3.4	2	284	340	D

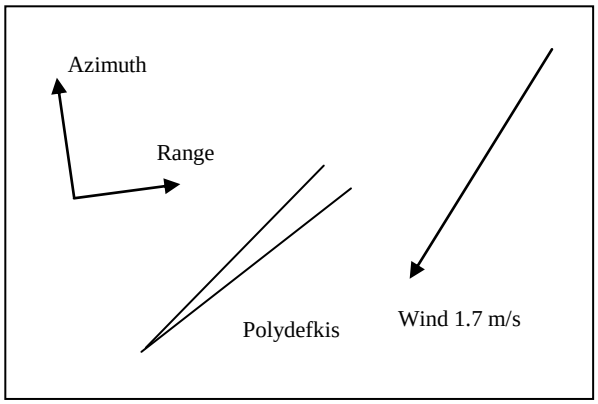

Fig. 7. Geometry of Polydefkis.

In the absence of evidence to the contrary and for builds prior to 2000, it was assumed that a single screw ship was probably propelled by a right-handed screw. The hydrodynamic modulation model implies that a right-handed propeller is associated with a bright wake edge on the starboard side while a bright edge on the port side is associated with a left-handed propeller. These areas are where Bragg waves entering or exiting the wake are decelerated and compressed.

Using this data, a simple diagram of each situation can be constructed as shown in Fig. 7. The cargo ship "Polydefkis" has one screw and the flow on the starboard side of the wake is expected to be outwards. However the Bragg directions are parallel to the range. The principal Bragg waves, which are in the direction of the Bragg waves with the greatest amplitude, will be towards the radar; waves will enter the wake from the port side with a small velocity component in the same direction as the swirl flow and exit from the starboard side. Therefore ambient waves may be affected only slightly by the swirl flow and no visible wake may occur. This behavior is more or less consistent with the simulations based on the Swanson model [10,12].

A similar explanation may apply to the Algowood, which has a left handed screw [34], the Blacky and the Hebron Sea. The last of these is also traveling quite slowly. The Grand Mariner is a passenger ship and probably excites swirl flows that are too weak because it is so small. In contrast, it is not obvious why the wakes from the Stella Prima and the National Geographic Explorer were not visible. There is a possibility that their propellers were too deep to create sufficiently strong surface flows.

The wakes from ships with two screws tended to be visible no matter from which direction the wind blew or the principal Bragg wave direction. Out of the 16 visible wakes, bright wake edges were observed on the starboard side in 13 cases and on the port side in 3 cases.

On the other hand, of the 15 ships with a single screw, 3 ships produced visible wakes that were difficult to interpret; 7 exhibited visible bright lines only on the starboard side, 3 only on the port and 2 on both starboard and port. The last of these were identified tentatively as narrow-V wakes and the ships were traveling close to the azimuthal direction.

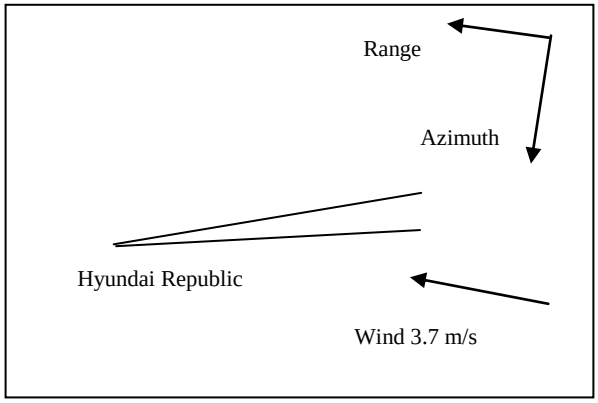

Fig. 8. Geometry of Hyundai Republic.

Table 5 summarizes an analysis of the bright wake arms with respect to wind direction. If the wind was blowing on the side of the wake with the bright arm, the wake was included in the "Same" column. Here, the dark wake, narrow-V wakes and uncertain cases, such as head and following winds, were included in the "Uncertain" column.

The results for single screw ships are inconclusive but for twin screw vessels it is clear that there is a strong tendency for the bright arm to occur on the side on which the wind blows. The exception in the second row is due to the cruise ship, the Crystal Symphony, which was traveling from New York to Montreal

with a stop at Halifax. This was observed beginning its turn towards Halifax harbor and was probably driven primarily by its starboard propeller. In this context, it can probably be regarded as a single propeller ship; the bright arm was on the starboard side and the wind was from the port side. With this exception, the second row is consistent with the hydrodynamic modulation mechanism above the 99% level of significance.

TABLE 5
WIND DIRECTION SIDE ANALYSIS

Screws	Same	Opposite	Uncertain
1	5	4	6
2	12	1	3

To reconcile the situation for single screw ships, we examined the screw handedness. The wakes can be divided according to whether the bright arm lies on the side of the wake where swirling flow accelerates or decelerates Bragg waves entering or exiting the flow. For example, the wake of the Canadian Prospector exhibited a bright line on the starboard side. This ship was built in 1963 and Seaway Marine Transport of St. Catherines, Ontario, has confirmed that it has a fixed pitch propeller [34]. Assuming that the screw is right-handed, this wake contributes to the "Decelerates" column of Table 6.

There were three ships that exhibited a bright line on the port side. One was the Queen of Alberni, which is a double ended ferry and could have been under way using its left handed CPP. The Captain Henry Jackman was a second. This has a left-handed CPP [34].

The third ship which exhibited a bright arm only on the port side was the Hyundai Republic, which was built in 2001. Fig. 8 shows the geometry. The direction of the wind implies that Bragg waves were predominately westward towards the ship stern and approaching on the port side. It is possible that the propeller linear-momentum wake, flowing almost in the opposite direction to the wind vector was responsible for the bright line on the port side. Presently, the rotation direction of the screw is not known; it could be left-handed.

If we correct the ratio 7:3 for the two cases of a left-handed screw, the ratio of wakes consistent with the modulation model becomes 9:1; relative to the null hypothesis in which the bright side of the wake is independent of the screw handedness, this is significant at about the 97% level.

In Table 6, narrow-V wakes and wakes that were difficult to interpret were again included as "Uncertain".

TABLE 6
BRIGHT ARM FLOW ANALYSIS (SINGLE SCREW)

Accelerates	Decelerates	Uncertain
1	9	5

The difference between the observations for single screw ships in the two tables implies that the wind can not only generate Bragg waves on the ambient sea that enter the wake and are compressed but also within the wake. The latter then exit the wake on the same side but in the opposite direction and are compressed similarly. Therefore the direction of the wind is not critical. However, the fact that the wakes of twin screw vessels tend to exhibit bright arms on the side on which the wind blows suggests that Bragg waves entering the wake dominate those exiting.

VIII. CONCLUSIONS

The observations of RADARSAT-2 ship wakes with AIS, though limited to only 60 ships, strongly suggest the following:

1. Wind speed is the main factor in turbulent wake visibility; above speeds of 6 m/s, these wakes are usually not visible but, below this threshold, there is a strong likelihood of a visible wake.
2. Wake visibility is enhanced at high ship speeds. If the wind speed is less than 6 m/s and the ship speed is greater than 5 m/s, the turbulent wake is visible with a probability of more than 80%.

Bright wake arms were observed more frequently than reported by other workers [15]; this may be due to the use of dual rather than single polarized imagery.

Turbulent wakes from ships with twin counter-rotating screws usually exhibit a bright line on the side of the wake on to which the wind is blowing. The bright line in wakes from single screw ships that are moving ahead usually lies on the starboard side of the wake when the propeller is right-handed and on the port side when it is left-handed.

The observations are consistent with a hydrodynamic modulation model based primarily on flows from propeller swirl. Linear flows could also be important under some conditions.

In conjunction with AIS and other information, the study also suggests that radar wakes can provide useful confirmation of ship propulsion characteristics in particular the sense of rotation of the propellers.

A larger database of ships and wakes and a comprehensive model of radar ship wakes are desirable to predict the wake characteristics from combined swirling and linear flows for vessels with both single and twin screws. This model could augment ship surveillance programs and contribute towards maritime security.

REFERENCES

[1] J.K.E. Tunaley, Algorithms for Ship Detection and Tracking Using Satellite Imagery, Proc. Geoscience and Remote Sensing Symposium, IGARSS 2004, Anchorage, Alaska, vol. 3, pp 1804-1807, September, 2004.

[2] J. Lighthill, Waves in Fluids, Cambridge University Press, 1978.

[3] K. Case, C. Callan, R. Dashen, R. Davis, W.Munk, J.Vesecky, K. Watson, F. Zachariasen, SEASAT III and IV, Report JSR-84-203, JASON, MITRE Corporation, 1820 Dolley Madison Boulevard, McLean, Virginia 22102, August 1984.

[4] J. W. Wright, "Backscattering from capillary waves with application to sea clutter." IEEE ***Trans. Ant. Prop.*** vol AP-14, pp 749-754, 1966.

[5] J.W. Wright, A New Model for Sea Clutter, IEEE Trans. Ant. Prop., vol. AP-16(2), pp 217-223, 1968.

[6] E.H. Buller and J.K.E. Tunaley, The effect of the ships screws on the ship wake and its implication for the radar image of the wake. Proc. IGARSS 89, Victoria, B.C. Canada, pp. 362-365, 1989.

[7] J.K.E. Tunaley, E.H. Buller, K.H. Wu and M.T. Rey, The Simulation of the SAR Image of a Ship Wake, IEEE Trans. Geoscience and Remote Sensing, vol. 29(1), pp 149-156, 1991.

[8] R.D. Peltzer, W.D. Garrett and P.M. Smith, A Remote Sensing Study of a Surface Ship Wake, IEEE Proc. Oceans 1984, vol. 17, pp 277-286, 1984.

[9] J.D. Lyden, D.R. Lyzenga, R.A. Shuchman and C.V. Swanson, SAR Detection of Ship-Generated Turbulent and Vortex Wakes, Environmental Research Institute of Michigan Report RR-86-112, 1986.

[10] A. Skoelv, Simulations of SAR Imaging of Ship Wakes, Comparing Different Wind Growth Models, Norwegian Defence Establishment Report, FFI/NOTAT-90/7054, 1990.
[11] A. Skoelv, Simulations of SAR Imaging of Ship Wakes, Comparing Different Wind Growth Rate Models, IEEE Geoscience and Remote Sensing Symposium, IGARSS '91, vol. 2, pp 851-854, June, 1991.
[12] A. Skoelv and T. Wahl, SAR Imaging of Vortex Ship Wakes, Norwegian Defence Establishment Report, FFI/RAPPORT-91/7077, 1991.
[13] A Skoelv, T Wahl, and S Eriksen, Simulation of SAR Imaging of Ship Wakes, IEEE Geoscience and Remote Sensing Symposium, IGARSS '88, vol. 3, pp. 1525-1528, September, 1988.
[14] C.V. Swanson, Radar Observation of Ship Wakes, Cortana Corporation, Falls Church, Virginia, USA, 1984.
[15] A. Skoelv, ERS Detection of Soft and Hard Targets at Sea, ERS Applications, Proc. 2nd International Workshop, London, December, 1995.
[16] A.M. Reed and J.H. Milgram, Ship Wakes and Their Radar Images, Annual Rev. Fluid Mech, vol. 34, pp 469–502, 2002.
[17] I. Hennings, R. Romeiser, W. Alpers and A. Viola, Radar Imaging of Ship Wakes, Int. J. Remote Sensing, vol 20 (13), pp 2519-2543, 1999.
[18] C. Melsheimer, H. Lim, and C. Shen, Observation and Analysis of Ship Wakes in ERS-SAR and Spot Images, Proc. 20th Asian Conference on Remote Sensing, Hong Kong, China, pp 554-559, 1999.
[19] H.E. Saunders, Hydrodynamics in Ship Design, vols. 1 & 2, SNAME, N.Y., 1957.
[20] D. Gerr, *Propeller Handbook*, International Marine, Camden, Maine, 2001.
[21] M. Collins and G. Peterson, Investigation of a Propulsion System Failure on a Large Double End Ferry, BC Ferries Report, 2007, http://www.tekna.no/ikbViewer/Content/19905/Collins-Peterson%20DEF%202007a.pdf
[22] J.P. Comstock (ed.), Principles of Naval Architecture, SNAME, N.Y., 1967.
[23] H. Schlichting, *Boundary Layer Theory*, McGraw-Hill, 1979.
[24] G. Birkhoff and E.H. Zarantonello, *Jets, Wakes and Cavities*, Academic Press, New York, 1957.
[25] A.J. Reynolds, Similarity in Swirling Wakes and Jets, Fluid Mech., vol. 14, pp 241-243, 1961.
[26] H. Higuchi and T. Kubota, Axisymmetric Wakes behind a Slender Body Including Zero-Momentum Configurations, Physics of Fluids A, vol. 2(9), pp 1615-1623, 1990.
[27] A.I. Serviente and V.C. Patel, Experiments in the Turbulent Near Wake of an Axisymmetric Body, AIAA Journal, Vol. 37(12), pp 1670-1773, 1999.
[28] A.I. Serviente and V.C. Patel, Wake of a Self-Propelled Body, Part 1: Momentumless Wake, AIAA Journal, Vol. 38(4), pp 613-619, 2000.
[29] E. Naudascher, Flow in the wake of self-propelled bodies and related sources of turbulence. J. Fluid Mech., vol. 22(4), pp 635-656, 1965.
[30] A.I. Serviente and V.C. Patel, Wake of a Self-Propelled Body, Part 2: Momentumless Wake with Swirl, AIAA Journal, Vol. 38(4), pp 620-627, 2000.
[31] G.G. Chernykh, A.G. Demenkov and V. A. Kostomakha, Swirling turbulent wake behind a self-propelled body, International Journal of Computational Fluid Dynamics, Vol. 19, No. 5, July 2005, 399–408.
[32] A.C.M. Stoffelen and D.L.T. Anderson, Scatterometer data interpretation: measurement and inversion, J. Atmos. And Oceanic Technology, Vol. 14(6), pp 1298-1313, 1997.
[33] A. Harati-Mokhtari., A. Wall, P. Brooks and J. Wang, "Automatic Identification System (AIS): A Human Factors Approach". The Nautical Institute AIS Forum, pp. 1-11, 2007.
[34] R. Armstrong, Seaway Marine Transport, St. Catherines, Ontario, Private Communication, February, 2010.